A Study of the Hydrogen Abstraction Reactions of C_2H Radical with CH_3CN, C_2H_5CN, and C_3H_7CN by Dual-Level Generalized Transition State Theory

Zeng-Xia Zhao, Jing-Yao Liu, Li Wang, Hong-Xing Zhang,* Chun-Yuan Hou, and Chia-Chung Sun

Institute of Theoretical Chemistry, State Key Laboratory of Theoretical and Computational Chemistry, Jilin University, Changchun 130023, People's Republic of China

Received: May 7, 2008; Revised Manuscript Received: June 26, 2008

The hydrogen abstraction reactions $C_2H + CH_3CN \rightarrow$ products (R1), $C_2H + CH_3CH_2CN \rightarrow$ products (R2), and $C_2H + CH_3CH_2CH_2CN \rightarrow$ products (R3) have been investigated by dual-level generalized transition state theory. Optimized geometries and frequencies of all the stationary points and extra points along the minimum-energy path (MEP) are performed at the BH&H-LYP and MP2 methods with the 6−311G(d, p) basis set, and the energy profiles are further refined at the MC-QCISD level of theory. The rate constants are evaluated using canonical variational transition state theory (CVT) with a small-curvature tunneling correction (SCT) over a wide temperature range 104−2000 K. The calculated CVT/SCT rate constants are in good agreement with the available experimental values. Our calculations show that for reaction R2, the α-hydrogen abstraction channel and β-hydrogen abstraction channel are competitive over the whole temperature range. For reaction R3, the γ-hydrogen abstraction channel is preferred at lower temperatures, while the contribution of β-hydrogen abstraction will become more significant with a temperature increase. The branching ratio to the α-hydrogen abstraction channel is found negligible over the whole temperature range.

Introduction

The ethynyl radical, C_2H, is of fundamentally important intermediate in combustion chemistry[1,2] and planetary atmosphere,[3−8] and the kinetics of it have attracted considerable attention. Furthermore, this radical plays an important part in the photochemistry of Tian's atmosphere,[9−11] and there is need to obtain the information of accurate rate constants and product branching ratios of chemical reactions involving C_2H radical in the lower temperature range, which is important to the accurate description of the photochemical models of Titan's atmospheres. Nitrogen-containing compounds such as hydrogen cyanide (HCN), cyanoacetylene, methyl cyanide (CH_3CN), and others have been identified as components of Titan's atmosphere,[12−14] and reactions of them with C_2H radicals play an important role in the synthesis of heavier molecules and understanding the formation of photochemical smog that is present in Titan's atmosphere. However, there are limited literature reports on the C_2H radical reactions with nitriles[15,16] compared to lots of investigation on reactions of C_2H radical with hydrocarbons.[17−25] The rate constants of C_2H reaction with methyl cyanide (CH_3CN) are determined in the temperature range of 262−360 K and 104−296 K by experiment.[15,16] For the reactions of C_2H with ethyl cyanide (C_2H_5CN) and propyl cyanide (C_3H_7CN), only one experiment is available in the temperature range 104−296 K reported by Nizamov and Leone.[15] However, these kinetic studies only provide the total rate constants. In the view of the mechanism only one hydrogen abstraction channel exists in the reaction of C_2H with CH_3CN, i.e., $C_2H + CH_3CN \rightarrow C_2H_2 + CH_2CN$ (R1) while for the reaction of C_2H with CH_3CH_2CN, C_2H radical can attack the hydrogen atom on the methylene group or the methyl group, i.e.,

$$C_2H + CH_3CH_2CN \rightarrow CH_3CHCN + C_2H_2 \quad \text{(R2a)}$$

$$C_2H + CH_3CH_2CN \rightarrow CH_2CH_2CN(C_s) + C_2H_2 \quad \text{(R2b-1)}$$

$$C_2H + CH_3CH_2CN \rightarrow CH_2CH_2CN(C_1) + C_2H_2 \quad \text{(R2b-2)}$$

Similarly, for the reaction of C_2H with $CH_3CH_2CH_2CN$ the hydrogen atom can be abstracted from α-, β-, and γ-carbon atoms, i.e.,

$$C_2H + CH_3CH_2CH_2CN \rightarrow CH_3CH_2CHCN + C_2H_2 \quad \text{(R3a)}$$

$$C_2H + CH_3CH_2CH_2CN \rightarrow CH_3CHCH_2CN + C_2H_2 \quad \text{(R3b)}$$

$$C_2H + CH_3CH_2CH_2CN \rightarrow CH_2CH_2CH_2CN(C_s) + C_2H_2 \quad \text{(R3c-1)}$$

$$C_2H + CH_3CH_2CH_2CN \rightarrow CH_2CH_2CH_2CN(C_1) + C_2H_2 \quad \text{(R3c-2)}$$

Up to now, no experimental information is available on the branching ratios of the above reactions, since it is difficult to determine which hydrogen atom is abstracted in experiments. Therefore, theoretical investigations are very desirable to give a deeper understanding on mechanisms of the title reactions.

In this paper, we employ dual-level generalized transition state theory (X//Y)[26] to study the above reactions. In this methodology, the information on the reaction path profiles is obtained directly from *ab initio* and density functional theory (DFT) electronic structure calculations. Subsequently, by means of the Polyrate 8.4.1 program the rate constants are calculated by

* To whom correspondence should be addressed.

10.1021/jp804010t CCC: $40.75
Published on Web 08/16/2008

variational transition state theory (VTST)[27−29] proposed by Truhlar and co-workers for each reaction channel. The calculated results are compared with available experimental results.

It is well-known that the knowledge of the standard enthalpy of formation of the species is important in determining the thermodynamic properties and the kinetics of the atmospheric process as well as stability of intermediate complexes and the feasible reaction paths. However, there is no thermodynamic data available to most of the reactants and products involved in the title reactions. In the present study, we attempt to estimate the enthalpies of formation for these species via isodesmic reactions.

Calculation Methods

The geometries and frequencies of all the stationary points, including reactants, products, and transition states (TSs) are optimized by using both Beck's half an d-half (BH&H)[30] nonlocal exchange and the Lee−Yang−Parr[31] nonlocal correlation functionals (BH&H-LYP) and restricted or unrestricted second-order Møller−Plesset perturbation theory (MP2) with the 6−311G(d, p) basis set (i.e., BH&H-LYP/6−311G(d, p) and MP2/6−311G(d, p)). At the same level, the minimum energy path (MEP) is obtained by intrinsic reaction coordinate theory (IRC) to confirm that the transition state really connects the minima along the path. Also, first and second energy derivatives at geometries along the MEP are obtained to calculate the curvature of the reaction path and to calculate the generalized vibrational frequencies along the reaction path. To obtain more accurate and reliable reaction energies along the MEP, higher level single point calculations are performed at the multicoefficient correlation method based on quadratic configuration interaction with single and double excitation (MC-QCISD)[32] level of theory using the BH&H-LYP and MP2 optimized geometries. For simplicity, hereinafter they are denoted by MC-QCISD//BH&H-LYP and MC-QCISD//MP2. All of above calculations are carried out by Gaussian 98 program package.[33]

By means of the Polyrate 8.4.1 program,[34] the rate constants are calculated by using the variational transition-state theory (VTST) proposed by Truhlar and co-workers. The level of VTST that we used is canonical variational transition-state theory (CVT) with the small-curvature tunneling (SCT) approximation.[35,36] The curvature components are calculated by using a quadratic fit to obtain the derivative of the gradient with respect to the reaction coordinate. Finally, the total rate constants are obtained from the sum of the individual rate constants.

The isodesmic reaction,[37] in which the number and type of bonds are conserved, will cancel the systematic errors in the calculations and lead to quite accurate results because of the similarity of bond type in both the reactants and products. This property makes isodesmic reactions a valuable tool for the prediction of heats of formations. In order to evaluate the heats of formation ($\Delta H^0_{f,298}$) of the species that have been little studied experimentally, we performed the calculation at MC-QCISD//BH&H-LYP/6−311G(d, p) and MC-QCISD//MP2/6−311G(d, p) levels using the following isodesmic reactions,

$$CH_3CN + CH_4 \rightarrow HCN + CH_3CH_3 \quad (R4)$$

$$CH_2CN + CH_4 \rightarrow CH_3CN + CH_3 \quad (R5)$$

$$CH_3CH_2CN + CH_4 \rightarrow CH_3CN + CH_3CH_3 \quad (R6)$$

$$CH_3CHCN + CH_4 \rightarrow CH_2CN + CH_3CH_3 \quad (R7)$$

$$CH_2CH_2CN(C_s) + CH_4 \rightarrow CH_3CN + CH_2CH_3 \quad (R8)$$

$$CH_2CH_2CN(C_1) + CH_4 \rightarrow CH_3CN + CH_2CH_3 \quad (R9)$$

$$CH_3CH_2CH_2CN + CH_4 \rightarrow CH_3CN + CH_3CH_2CH_3 \quad (R10)$$

$$CH_3CH_2CHCN + CH_4 \rightarrow CH_3CN + CH_3CHCH_3 \quad (R11)$$

$$CH_3CHCH_2CN + CH_4 \rightarrow CH_3CN + CH_3CHCH_3 \quad (R12)$$

$$CH_2CH_2CH_2CN(C_s) + CH_4 \rightarrow CH_3CN + CH_3CHCH_3 \quad (R13)$$

$$CH_2CH_2CH_2CN(C_1) + CH_4 \rightarrow CH_3CN + CH_3CHCH_3 \quad (R14)$$

Results and Discussion

1. Stationary Points. The optimized geometric parameters of the reactants and products calculated at the BH&H-LYP and MP2 levels with the 6−311G(d, p) basis set are depicted in Figure 1 as well as the experimental values. It can be found that the optimized parameters obtained by the two levels are consistent with each other, and they agree well with the experimental values when the comparison is available. As shown in Figure 1, methyl cyanide (CH_3CN) is C_{3v} symmetry, ethyl cyanide (C_2H_5CN) and propyl cyanide (C_3H_7CN) are C_S symmetry, and CH_2CH_2CN and $CH_2CH_2CH_2CN$ radicals have two conformations with C_1 and C_s symmetries, respectively.

The optimized geometries of transition states are plotted in Figure 2. Since all three hydrogen atoms at the α-position of CH_3CN are equivalent, only one hydrogen abstraction channel has been located. The two hydrogen atoms at the α-position of CH_3CH_2CN are equivalent; only one α-hydrogen abstraction channel R2a via TS2a is located. As to the three β-hydrogen atoms in CH_3CH_2CN, H′ (in Figure 1) are different from the other two; as a result, two different β-hydrogen abstraction channels R2b-1 and R2b-2 are identified, leading to the products CH_2CH_2CN with C_s and C_1 symmetries, respectively. Consequently, there are three possible channels in the C_2H + CH_3CH_2CN reaction, that is, one α-hydrogen abstraction and two β-hydrogen abstractions. The three reaction channels are denoted by R2a, R2b-1, and R2b-2, respectively. Similarly, four hydrogen abstraction channels are found for the reaction C_2H + $CH_3CH_2CH_2CN$, i.e., one α-hydrogen abstraction reaction, one β-hydrogen abstraction, and two γ-hydrogen abstraction channels. They are denoted as R3a, R3b, R3c-1, and R3c-2, respectively. From above analysis, it has been shown that the number of possible transition states for the hydrogen abstraction channel of the C_2H reaction with R-CN will increase as the size of R increases. For the TSR1, the breaking C−H bond is elongated by both 6% at the BH&H-LYP and MP2 levels compared to the C−H equilibrium bond length of molecular CH_3CN, and the forming C−H bond is 58% and 48% longer than the C−H equilibrium bond length in isolated C_2H_2, respectively, which indicates that R1 proceeds via an early transition state. Similarly, other transition states involved in the title reactions also proceed via early transition states.

Table 1 gives the harmonic vibrational frequencies of the reactants and products calculated at the BH&H-LYP/6−311G(d, p) and MP2/6−311G(d, p) levels. The corresponding values for the transition states are listed in the Supporting Information. For comparison, the available experimental values are also given in the table.[38] Good agreement is obtained for most of calculated

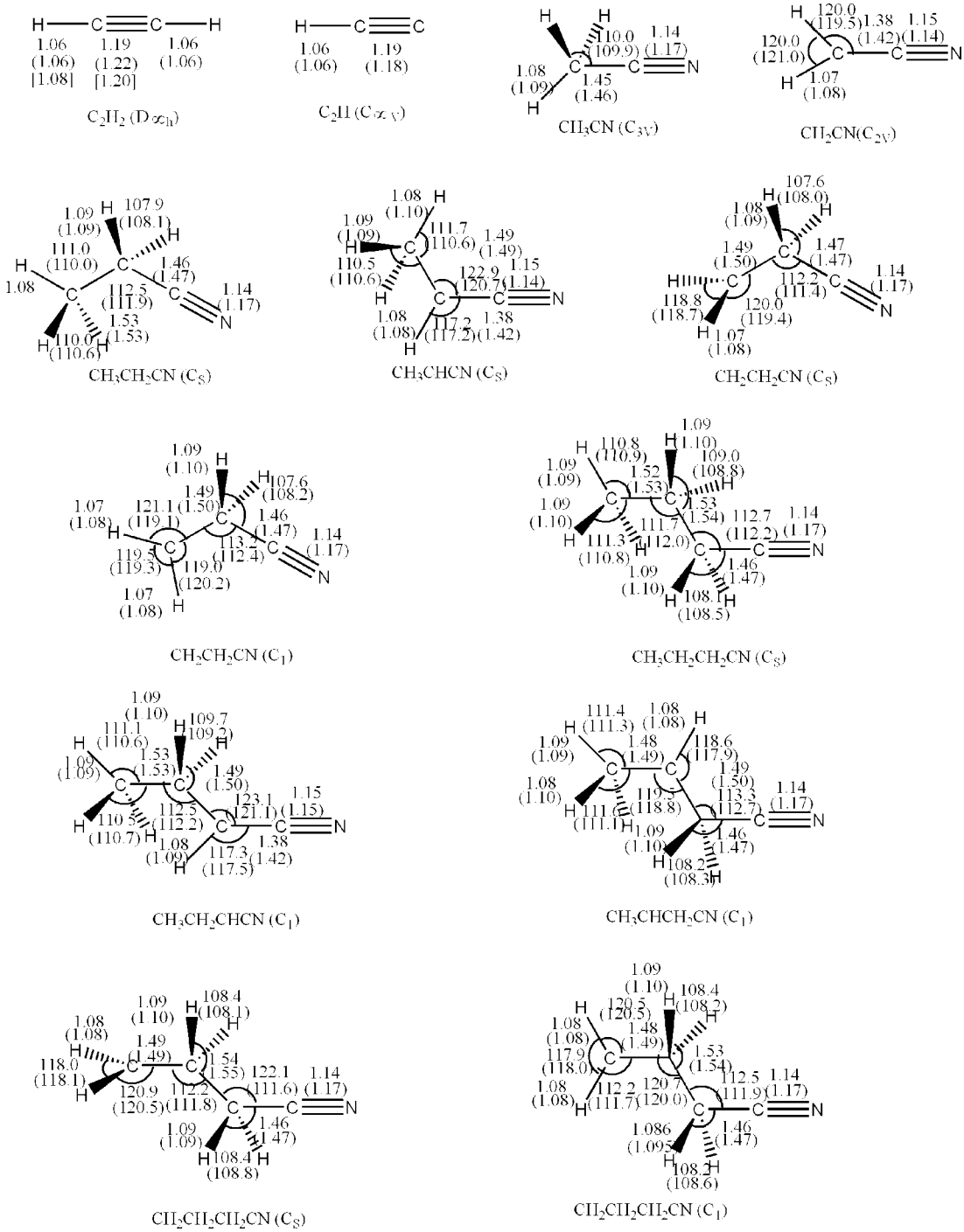

Figure 1. Optimized geometries of reactants and products at the BH&H-LYP/6−311G(d, p) and MP2/6−311G(d, p) (in parentheses) levels. The numbers in square brackets are the experimental values. Bond lengths are in angstroms and angles are in degrees.

frequencies within the maximum error around 10%. The transition state is identified with only one negative eigenvalue of the Hessian matrix. The imaginary frequencies of TSR1 are 243i and 515i at the BH&H-LYP and MP2 levels, respectively.

Because of the conservation of the number of electron pairs in the reactants and products the changes in their correlation energies are usually small, so that the reaction energies of isodesmic reactions can be predicted quite accurately with relatively cheap theoretical methods. Enthalpies of formation (ΔH^0_{298}) of the CH_3CN, CH_2CN, CH_3CH_2CN, CH_3CHCN, CH_2CH_2CN, $CH_3CH_2CH_2CN$, CH_3CH_2CHCN, CH_3CHCH_2CN, and $CH_2CH_2CH_2CN$ are evaluated by using the calculated reaction enthalpies of the isodesmic reactions and the experimental ΔH^0_{298} of the other species involved in the reactions. The known heats of formation of the reference compounds in these reactions (CH_4, −17.90 kcal/mol; CH_3, 34.84 kcal/mol; CH_3CH_3, −20.04 ± 0.07 kcal/mol; CH_3CH_2, 28.33 ± 0.48 kcal/mol; $CH_3CH_2CH_3$, 22.6 ± 3.24kcal/mol; CH_3CHCH_3, 21.43 ± 0.48kcal/mol; CH_3CN, 18.00 ± 3.00 kcal/mol; CH_2CN, 58.50 ± 3.00 kcal/mol; HCN, 32.30 kcal/mol)[38] are combined with these reaction (R4−R14) theoretical enthalpies to calculate the enthalpies of formation for the target species. The calculated ΔH^0_{298} values for the above species at the MC-QCISD//BH&H-LYP/6−311G(d, p) and MC-QCISD//MP2/6−311G(d, p) levels are tabulated in Table 2. The calculated enthalpies for each species show good consistency at two levels. In addition, the

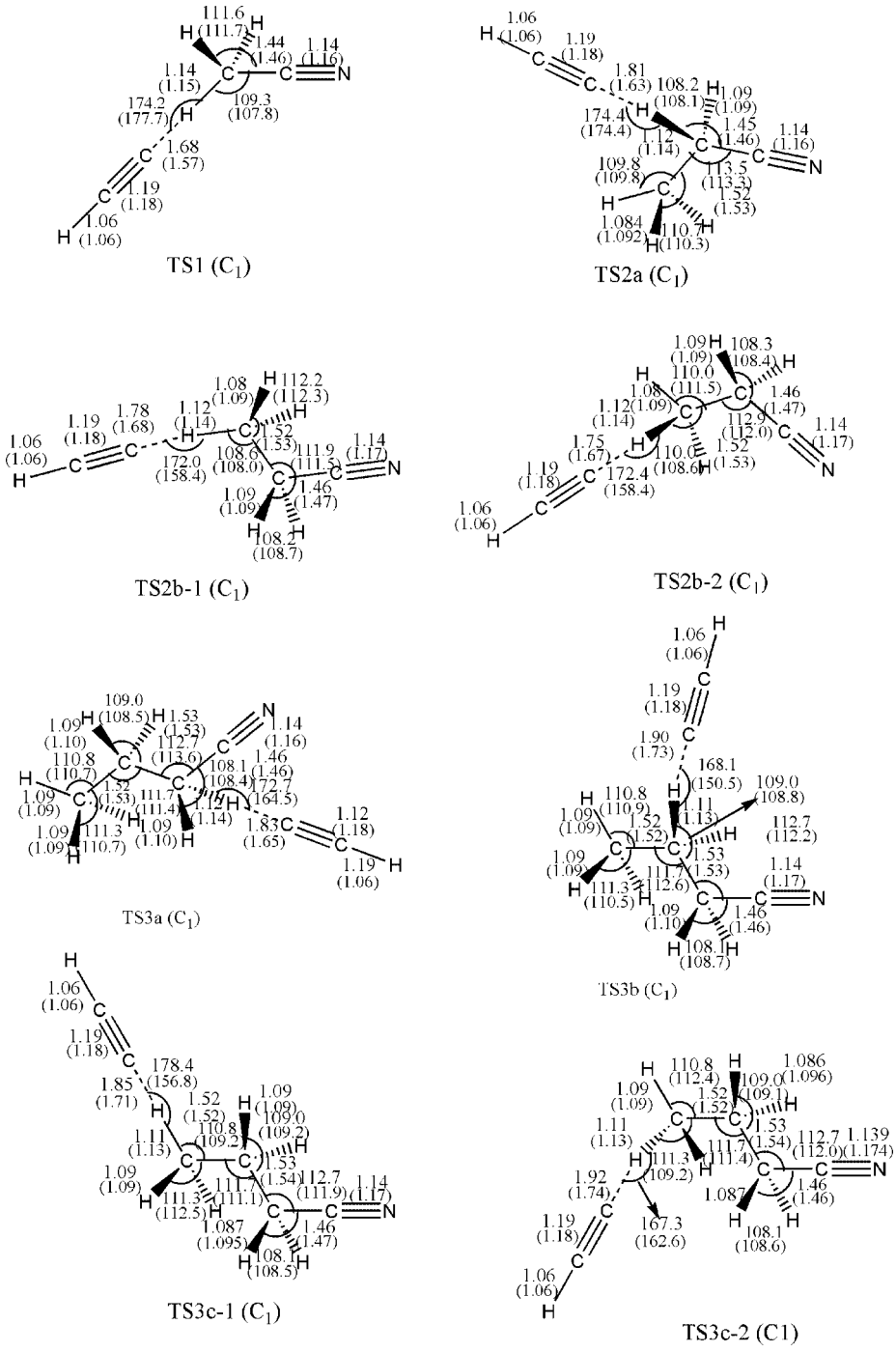

Figure 2. Optimized geometries of the transition states at the BH&H-LYP/6−311G(d, p) and MP2/6−311G(d, p) levels for all the reactions. Bond lengths are in angstroms, and angles are in degrees.

unweighted averaged calculated enthalpy values of 19.03 ± 0.18 kcal/mol for CH_3CN and 63.85 ± 3.63 kcal/mol for CH_2CN agree well with the experimental values 18.00 ± 3.00 and 58.50 ± 3.00 kcal/mol, respectively.[38] So it can be expected that the same accuracy can be obtained for other species at the same levels with the isodesmic reactions. Note that the error limits are calculated by adding the maximum uncertainties of ΔH^0_{298} values of the reference compounds taken from the literature.

The reaction enthalpies (ΔH^0_{298}) calculated at the BH&H-LYP/6−311G(d, p), MP2/6−311G(d, p), MC-QCISD//BH&H-LYP/6−311G(d, p), and MC-QCISD//MP2/6−311G(d, p) levels of theory are listed in Table 3. It is seen that results calculated by MC-QCISD//BH&H-LYP/6−311G(d, p) and MC-QCISD//MP2/6−311G(d, p) levels show good mutual agreement. Moreover, for the $C_2H + CH_3CN$ reaction, the reaction enthalpy values of −38.04 and −38.75 kcal/mol calculated at the MC-QCISD//BH&H-LYP/6−311G(d, p) and MC-QCISD//MP2/6−311G(d, p) levels, respectively, are in reasonable agreement with the experimental values of −40.15 ± 7.00 kcal/mol, which are derived from the experimental standard heats of formation (CH_3CN, 18.00 ± 3.00 kcal/mol; CH_2CN, 58.50 ± 3.00 kcal/mol; C_2H_2, 54.35 kcal/mol; C_2H, 135.00 ± 1.00 kcal/mol). Since the calculated enthalpy of reaction R1 agrees well with the experimental value[15] it can be inferred that the reaction enthalpies performed at these two levels are reliable. Furthermore, if we use the calculated enthalpy values in the above section as the $\Delta H^0_{f,298}$ of the reactants and products along with the experimental standard heats of formation (CH_3CN, 18.00

TABLE 1: Calculated Frequencies (in cm^{-1}) of the Stationary Points at the BH&H-LYP and MP2 Level (in Parentheses)

species	BH&H-LYP/6−311G(d, p) (MP2/6−311G(d, p))	expt
CH_3CN	408, 408, 960, 1105, 1105, 1466, 1527, 1528, 2489, 3138, 3215, 3215 (367, 367, 934, 1072, 1072, 1426, 1501, 1501, 2218, 3103, 3198, 3198)	362, 362, 920, 1041, 1041, 1381, 1448, 1448, 2266, 2954, 3009, 3009
C_2H	615, 618, 2165, 3550 (838, 838, 2471, 3577)	1848, 3612
CH_2CN	409, 459, 684, 1073, 1079, 1495, 2260, 3251, 3362 (429, 452, 576, 1020, 1076, 1471, 2754, 3246, 3374)	367, 437, 680, 1041, 1124, 2156, 3301
C_2H_2	727, 727, 818, 818, 2148, 3504, 3613 (561, 561, 769, 769, 1969, 3461, 3550)	640, 640, 730, 730, 1974, 3289, 3374
CH_3CH_2CN	224, 229, 416, 577, 819, 870, 1056, 1138, 1160, 1340, 1408, 1474, 1530, 1550, 1558, 2480, 3131, 3139, 3173, 3205, 3210 (208, 232, 383, 539, 799, 854, 1043, 1111, 1128, 1307, 1366, 1434, 1496, 1521, 1526, 2204, 3091, 3103, 3152, 3185, 3190)	222, 226, 378, 545, 786, 836, 1005, 1022, 1077, 1256, 1319, 1387, 1433, 1465, 1465, 2254, 2849, 2900, 2955, 3001, 3001
CH_3CHCN	75, 234, 442, 601, 606, 884, 1038, 1139, 1178, 1433, 1462, 1527, 1546, 2221, 3099, 3145, 3213, 3274	
CH_2CH_2CN (C_S)	39, 218, 391, 499, 617, 807, 931, 1097, 1132, 1331, 1369, 1509, 1520,2474, 3131, 3173, 3239, 3355	
CH_2CH_2CN (C_1)	78, 231, 382, 452, 583, 854, 923, 1079, 1130, 1257, 1405, 1504, 1510, 2485,3072, 3125, 3245, 3365	
$CH_3CH_2CH_2CN$	102, 175, 253, 361, 414, 560, 771, 908, 914, 991, 1087, 1159, 1175, 1309, 1358, 1379, 1447, 1475, 1528, 1548, 1554, 1563, 2479, 3111, 3126, 3135, 3152, 3168, 3187, 3188	
CH_3CH_2CHCN	35, 193, 265, 352, 442, 582, 628, 796, 912, 1030, 1099, 1143, 1197, 1322, 1370, 1466, 1470, 1533, 1550, 1557, 2220, 3083, 3117, 3165, 3189, 3193, 3264	
CH_3CHCH_2CN	52, 108, 177, 338, 368, 407, 560, 913, 922, 998, 1036, 1150, 1183, 1257, 1345, 1450, 1474, 1509, 1529, 1536, 2484, 3049, 3057, 3113, 3118, 3189	
$CH_2CH_2CH_2CN$ (C_s)	19, 108, 177, 343, 413, 528, 560, 767, 891, 973, 1019, 1108, 1161, 1298, 1330, 1376, 1418, 1515, 1529, 1550, 2478, 3124, 3143, 3163, 3189, 3227, 3334	
$CH_2CH_2CH_2CN$ (C_1)	103, 129, 177, 366, 414, 500, 563, 769, 897, 992, 1034, 1116, 1152, 1242, 1346, 1362, 1444, 1517, 1536, 2480, 3057, 3135, 3143, 3179, 3226, 3334	

TABLE 2: Calculated Enthalpies of Formation at Various Levels (in kcal/mol)

	MC-QCISD//BH&H-LYP/6−311G(d, p)	MC-QCISD//MP2/6−311G(d, p)	average value and deviation	expt
CH_3CN	18.92 ± 0.07	19.14 ± 0.07	19.03 ± 0.18	18.00 ± 3.00
CH_2CN	63.22 ± 3.00	64.47 ± 3.00	63.85 ± 3.63	58.50 ± 3.00
CH_3CH_2CN	13.68 ± 3.07	13.65 ± 3.07	13.67 ± 3.09	
CH_3CHCN	50.51 ± 3.07	50.60 ± 3.07	50.56 ± 3.12	
CH_2CH_2CN (C_S)	63.75 ± 3.48	64.89 ± 3.43	64.32 ± 4.00	
CH_2CH_2CN (C_1)	57.69 ± 3.48	64.72 ± 3.48	61.21 ± 7.00	
$CH_3CH_2CH_2CN$	8.49 ± 3.12	8.46 ± 3.12	8.48 ± 3.14	
CH_3CH_2CHCN	49.81 ± 3.12	51.67 ± 3.12	50.74 ± 4.05	
CH_3CHCH_2CN	56.22 ± 3.12	57.58 ± 3.12	59.60 ± 3.80	
$CH_2CH_2CH_2CN$ (C_S)	59.05 ± 3.12	59.00 ± 3.12	59.03 ± 3.15	
$CH_2CH_2CH_2CN$ (C_1)	58.59 ± 3.12	58.57 ± 3.12	58.58 ± 3.13	

TABLE 3: Calculated Reaction Enthalpies (ΔH^0_{298}) (in kcal/mol) for the Reactions at Various Levels

	BH&H-LYP/ 6−311G(d,p)	MC-QCISD// BH&H-LYP/6−311G(d,p)	MP2/ 6−311G(d,p)	MC-QCISD//MP2/ 6−311G(d,p)	expt
$CH_3CN + C_2H \rightarrow CH_2CN + C_2H_2$	−40.97	−38.04	−38.84	−38.75	−40.15 ± 7.00
$CH_3CH_2CN + C_2H \rightarrow CH_3CHCN + C_2H_2$	−45.31	−41.92	−42.15	−41.31	
$CH_3CH_2CN + C_2H \rightarrow CH_2CH_2CN + C_2H_2$	−32.83	−31.24	−41.74	−33.90	
$CH_3CH_2CN + C_2H \rightarrow CH_2CH_2CN + C_2H_2$	−33.78	−38.56	−41.42	−34.27	
$CH_3CH_2CH_2CN + C_2 \rightarrow CH_3CH_2CHCN + C_2H_2$	−45.22	−41.88	−41.74	−41.95	
$CH_3CH_2CH_2CN + C_2 \rightarrow CH_3CHCH_2CN + C_2H_2$	−37.53	−35.76	−38.15	−34.85	
$CH_3CH_2CH_2CN + C_2 \rightarrow CH_2CH_2CH_2CN + C_2H_2$	−34.11	−32.63	−43.20	−35.59	
$CH_3CH_2CH_2CN + C_2 \rightarrow CH_2CH_2CH_2CN + C_2H_2$	−34.48	−33.09	−43.27	−35.81	

± 3.00 kcal/mol; CH_2CN, 58.50 ± 3.00 kcal/mol; C_2H_2, 54.35 kcal/mol; C_2H, 135.00 ± 1.00 kcal/mol), the reaction enthalpies for the R2a, R2b-1, and R2b-2 are −43.76 ± 7.17, −30.00 ± 7.21, and −33.22 ± 11.12 kcal/mol, respectively. The corresponding values for the reactions R3a, R3b, R3c-1, and R3c-2 are −38.37 ± 8.19, −29.51 ± 7.94, −30.08 ± 7.29, and −30.53 ± 7.27 kcal/mol, respectively. It can be found that these values are also well consistent with the calculated values.

The schematic reaction path profiles of the $C_2H + CH_3CN$ (R1), $C_2H + CH_3CH_2CN$ (R2), and $C_2H + CH_3CH_2CH_2CN$ (R3) reactions obtained at the MC-QCISD//BH&HLYP/6−311G(d, p) and MC-QCISD//MP2/6−311G(d, p) levels are plotted in Figure 3a−c. For reaction R1 only one reaction channel is located with the barrier height of 2.64 and 2.35 kcal/mol at the MC-QCISD//BH&H-LYP/6−311G(d, p) and MC-QCISD//MP2/6−311G(d, p) levels of theory, respectively. For

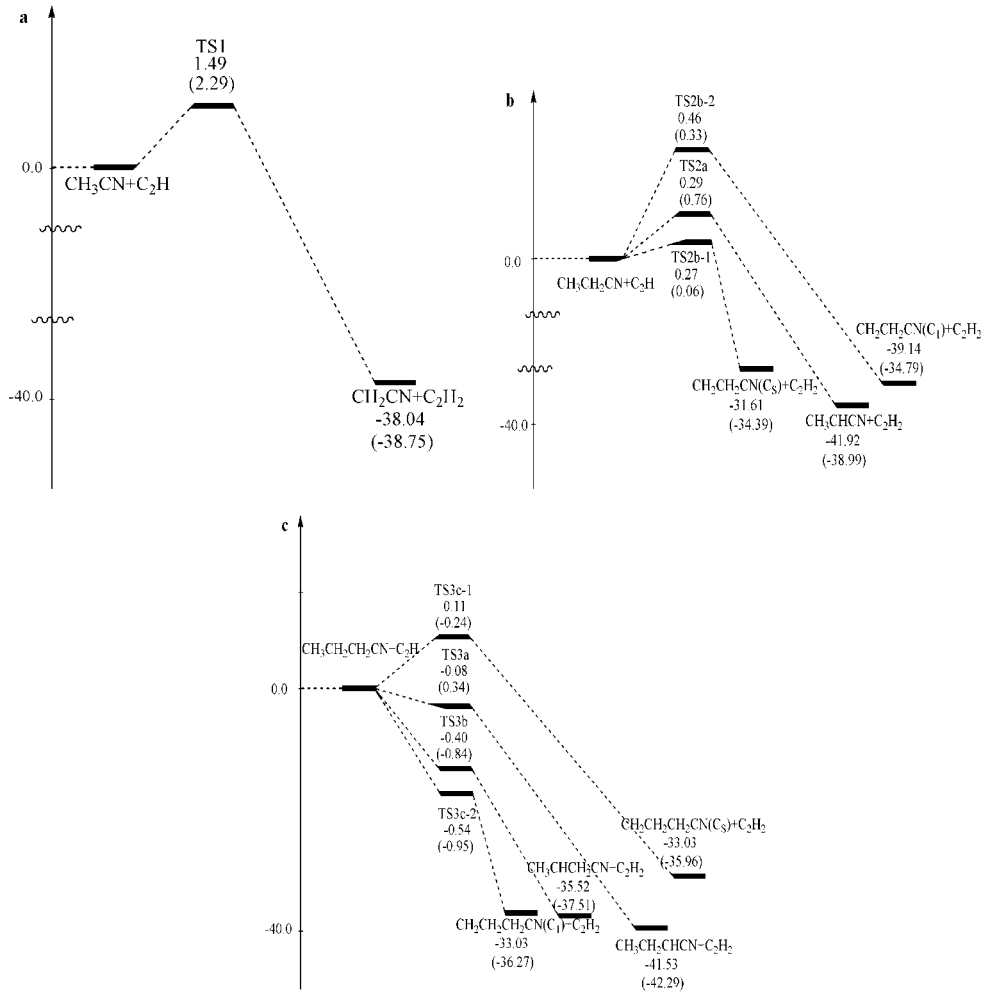

Figure 3. Schematic pathways for the reactions (a) $CH_3CN + C_2H$, (b) $CH_3CH_2CN + C_2H$, (c) $CH_3CH_2CH_2CN + C_2H$. Relative energies with ZPE at the MC-QCISD//BH&H-LYP/6−311G(d, p) level are in kcal/mol. The values in the parentheses are those obtained at the MC-QCISD//MP2/6−311G(d, p) level.

reaction R2, the barrier heights of R2a and R2b-1 are almost equivalent with the values of 0.29 and 0.27 kcal/mol at MC-QCISD//BH&H-LYP level, respectively. It can be predicated that α- and β-hydrogen abstraction channel are competitive for reaction R2. For reaction R3, the β-hydrogen abstraction channel R3b has the lowest barrier height with the value of −0.84 kcal/mol, which indicates that it will be the most favorite reaction path. The barrier height of γ-hydrogen abstraction (−0.54 kcal/mol) is slightly higher than that of β-hydrogen abstraction (−0.84 kcal/mol), so γ-hydrogen abstraction will also have some contribution to the total rate constants. Furthermore, their barrier heights are both lower than that of reaction R3a (−0.08 kcal/mol), i.e. β- and γ-position hydrogen are more reactive than the α-position hydrogen for reaction R3. The similar conclusion can be obtained at the MC-QCISD//MP2 level. The views will be further testified in the following study of the rate constants.

2. Minimum Energy Path. The MEP for each reaction is obtained by the intrinsic reaction coordinate (IRC) theory at the BH&H-LYP/6−311G(d, p) and MP2/6−311G(d, p) levels, and the potential profiles are further corrected at the MC-QCISD level. Since various properties along the MEP are similar for above the reactions, for brevity, we only take $C_2H + CH_3CN$ reaction as an example to discuss the reaction path features. The classical potential energy curve V_{MEP}, the vibrationally adiabatic ground-state potential energy curve V_a^G, and the zero-point energy (ZPE) curve as a function of the intrinsic reaction coordinate (s) are plotted in Figure 4, where $V_a^G(s) = V_{MEP}(s) + ZPE(s)$. It should be noted that the locations of the maximum on the $V_a^G(s)$ and $V_{MEP}(s)$ energy curves slightly shift in the s direction.[39] As can be seen, the $V_{MEP}(s)$ and $V_a^G(s)$ curves are similar shape, and the ZPE is practically constant as s varies, with only a gentle drop near the saddle point, which means that the variational effect is small.

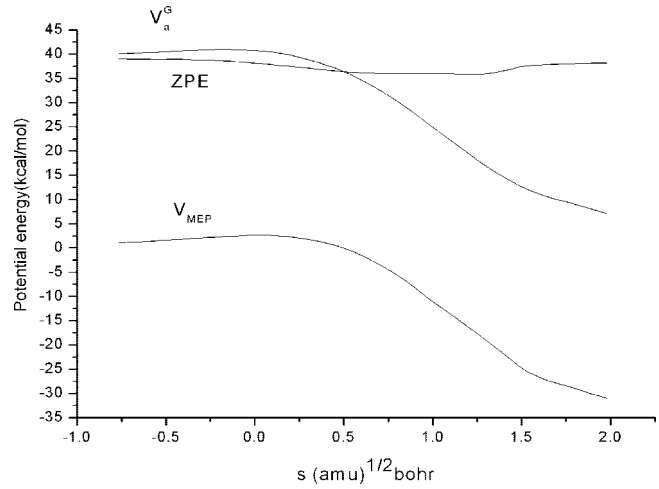

Figure 4. Classical potential energy curve (V_{MEP}), ground-state vibrationally adiabatic energy curve (V_a^G), and zero-point energy curve (ZPE) as functions of s (amu)$^{1/2}$ bohr at the MC-QCISD//BH&H-LYP/6−311G(d, p) level for the reaction $CH_3CN + C_2H$.

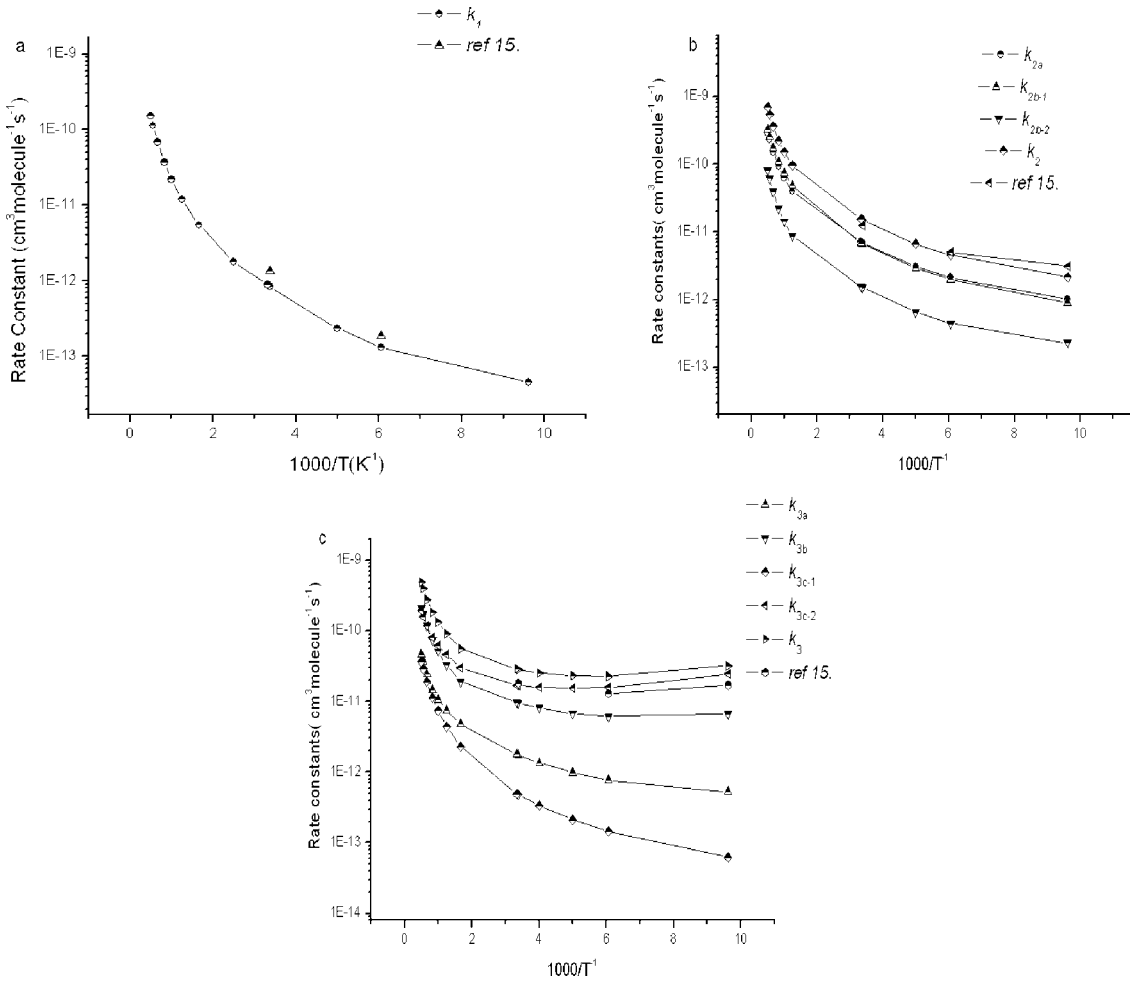

Figure 5. Plot of the CVT/SCT rate constants calculated at the MC-QCISD//BH&H-LYP/6−311G(d, p) level and the available experimental values versus 1000/T between 104 and 2000 K for the (a) $CH_3CN + C_2H$, (b) $CH_3CH_2CN + C_2H$, (c) $CH_3CH_2CH_2CN + C_2H$.

TABLE 4: Rate Constants (cm^3 molecule^{-1} s^{-1}) of R1, R2, and R3 for the Temperature Range 104−2000 K

T (K)	k_1	expt	k_2	expt	k_3	expt
104	4.16×10^{-14}		2.15×10^{-12}	$(4.10 \pm 0.80) \times 10^{-12}$	3.20×10^{-11}	$(1.30 \pm 0.40) \times 10^{-11}$
165	1.31×10^{-13}	$(1.50 \pm 0.40) \times 10^{-13}$	4.55×10^{-12}	$(4.80 \pm 0.90) \times 10^{-12}$	2.29×10^{-11}	$(1.50 \pm 0.40) \times 10^{-11}$
200	2.33×10^{-13}		6.62×10^{-12}		2.33×10^{-11}	
296	8.43×10^{-13}	$(1.35 \pm 0.30) \times 10^{-12}$	1.51×10^{-11}	$(1.05 \pm 0.20) \times 10^{-11}$	2.88×10^{-11}	$(1.80 \pm 0.30) \times 10^{-11}$
300	8.81×10^{-13}		1.56×10^{-11}		2.91×10^{-11}	
800	1.19×10^{-11}		9.62×10^{-11}		9.15×10^{-11}	
1000	2.20×10^{-11}		1.52×10^{-10}		1.33×10^{-10}	
1200	3.64×10^{-11}		2.23×10^{-10}		1.83×10^{-10}	
1500	6.76×10^{-11}		3.63×10^{-10}		2.79×10^{-10}	
1800	1.12×10^{-10}		5.46×10^{-10}		3.98×10^{-10}	
2000	1.50×10^{-10}		6.90×10^{-10}		4.90×10^{-10}	

3. Rate Constants. The rate constants for each reaction channel are calculated by using canonical variational transition states theory (CVT) with the small-curvature tunneling (SCT) correction at the MC-QCISD//BH&H-LYP/6−311G(d, p) level in the temperature range of 104−2000 K. The total rate constants are calculated as the sums of the corresponding individual rate constants, which are listed in Table 4, as well as available experimental values. Figure 5 displays the comparison of calculated rate constants to available experimental values. It can been seen that the calculated rate constants k_1, k_2, and k_3 are in good agreement with the experimental values reported by Nizamov et al. within a factor of 0.69−1.89. Furthermore, the Arrhenius expressions $k_1 = 9.25 \times 10^{-12} \exp(-713.68/T)$, $k_2 = 3.35 \times 10^{-11} \exp(-297.93/T)$, and $k_3 = 2.23 \times 10^{-11} \exp(28.10/T)$ fitted by the CVT/SCT rate constants in the temperature ranges of 165−360 K for reaction R1 and 104−296 K for reaction R2 and R3 are in good agreement with those reported by Nizamov and Leone,[15] $k_1 = (1.8 \pm 0.35 \times 10^{-11} \exp(-766 \pm 38/T)$, $k_2 = (1.5 \pm 0.3) \times 10^{-11} \exp(-145 \pm 10/T)$, and $k_3 = (2.1 \pm 0.4) \times 10^{-11} \exp(-51 \pm 38/T)$.

The temperature dependence of the k_{2a}/k_2 and k_{2b}/k_2 branching ratios are exhibited in Figure 6a, where $k_{2b} = k_{2b\text{-}1} + k_{2b\text{-}2}$. As shown in the Figure 6a we can see that the k_{2b} are slightly higher than k_{2a} over the whole temperature range, that is, α-hydrogen and β-hydrogen abstractions are competitive reaction channels. As to reaction R3 the k_{3c}, where $k_{3c} = k_{3c\text{-}1} + k_{3c\text{-}2}$, are 1−2 order larger than k_{3a} and k_{3b} and the total rate constants are nearly equal to that of reaction R3*c*. Thus, the γ-hydrogen abstraction channel is preferred in the lower temperatures; however, the contribution of the β-hydrogen abstraction to the

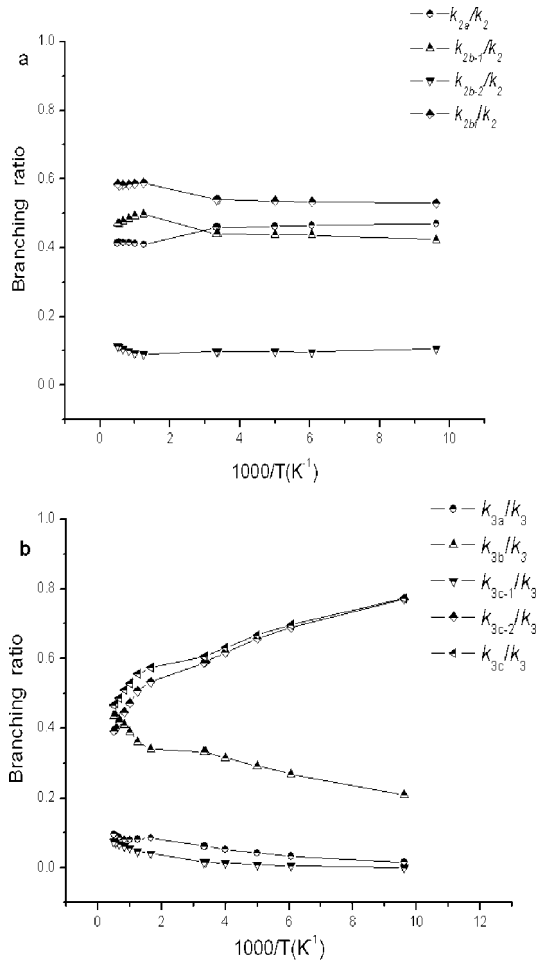

Figure 6. Plot of the calculated branching ratio versus 1000/T between 104 and 2000 K for the (a) $CH_3CH_2CN + C_2H$, (b) $CH_3CH_2CH_2CN + C_2H$.

total rate constants increases with the temperature increasing with the ratios of 26% at 104 K, 39% at 600 K, and 42% at 2000 K. It can be concluded that both γ- and β-hydrogen abstraction will contribute to the total rate constants in the higher temperatures. As to reaction R3a, the branching ratio of k_{3a}/k_3 ranges from 2% at 104 K to 12% at 2000 K, i.e., α-hydrogen abstraction channel has a minor contribution in the whole temperature range. This conclusion is consistent with the analysis in the above section.

Owing to the good agreement between the theoretical and experimental values, it is reasonable to believe that our calculated results will provide a good estimate for the kinetics of the reactions in the high temperature range. For convenience of future experimental measurements, the three-parameter fits for the CVT/SCT rate constants for the title reactions within 104−2000 K give the expressions as follows (in cm^3 molecule^{-1} s^{-1}):

$$k_1 = 1.09 \times 10^{-19} T^{2.77} \exp(-1.55/T)$$

$$k_2 = 8.90 \times 10^{-17} T^{2.08} \exp(-45.36/T)$$

$$k_3 = 8.19 \times 10^{-17} T^{2.02} \exp(-363.77/T)$$

Conclusion

In this paper, the hydrogen abstraction reactions $C_2H + CH_3CN \rightarrow$ products (R1), $C_2H + CH_3CH_2CN \rightarrow$ products (R2), and $C_2H + CH_3CH_2CH_2CN \rightarrow$ products (R3) have been studied by the dual-level generalized transition state theory at MC-QCISD//B3LYP/6−311G(d, p) and MC-QCISD//MP2/6−311G(d, p) levels. The rate constants calculated by canonical variational transition state theory with the small-curvature tunneling correction (CVT/SCT) agree well with the experimental constants. For reaction R2, the α- and β-hydrogen abstraction channels are competitive reaction channels. For reaction R3, γ-hydrogen abstraction is the predominant pathway in the lower temperature range; however, β-hydrogen abstraction becomes more important as the temperature increases. Then, both reaction channels contribute to the reaction. The three-parameter expressions (in cm^3molecule^{-1} s^{-1}) for three reactions within 104−2000 K are $k_1 = 1.09 \times 10^{-19} T^{2.77} \exp(-1.55/T)$, $k_2 = 8.90 \times 10^{-17} T^{2.08} \exp(-45.36/T)$, and $k_3 = 8.19 \times 10^{-17} T^{2.02} \exp(-363.77/T)$. Considering the absence of experimental rate data for higher temperatures, we hope that the present theoretical results are useful and reasonable to estimate the dynamical properties of these reactions over a wide temperature range.

Acknowledgment. We thank Professor Donald G. Truhlar for his provision of the POLYRATE 8.4.1 program. This work is supported by the National Natural Science Foundation of China (20573042, 20073014), Doctor Foundation by the Ministry of Education, and Foundation for University Key Teacher by the Ministry of Education, Key Subject of Science and Technology by the Ministry of Education of China, and Key Subject of Science and Technology by Jilin Province.

Supporting Information Available: Tables containing the results from the BH&H-LYP/6−311G(d, p) and MP2/6−311G(d, p) calculations of frequencies of transitions states. This information is available free of charge via the Internet at http://pubs.acs.org.

References and Notes

(1) Shaub, W. M.; Bauer, S. H. *Combust. Flame* **1978**, *32*, 35.
(2) Devriendt, K.; Peeters, J. *J. Phys. Chem. A* **1997**, *101*, 2546.
(3) Jackson, W. M. Y. H. B.; Urdahl, R. S. *J. Geophys. Res., [Planets]* **1991**, *96*, 17569.
(4) Tucker, K. D.; Kutner, M. L.; Thaddeus, P. *J. Astrophys.* **1974**, *193*, L115.
(5) Hasegawa, T. I.; Kwok, S. *J. Astrophys.* **2001**, *562*, 824.
(6) Markwick, A. J.; Ilgner, M.; Millar, T. J.; Henning, T. *Astron. Astrophys.* **2002**, *385*, 632.
(7) Strobel, D. F. *Planet. Space Sci.* **1982**, *30*, 839.
(8) Allen, M.; Yung, Y. L.; Gladstone, G. R. *Icarus* **1992**, *100*, 527.
(9) Lara, L. M.; Lellouch, E.; LopezMoreno, J. J.; Rodrigo, R. *J. Geophys. Res., [Planets]* **1996**, *101*, 23261.
(10) Toublane, D.; Parisot, J. P.; Brillet, J.; Gautier, D.; Raulin, F.; McKay, C. P. *Icarus* **1995**, *117*, 218.
(11) Yung, Y. L.; Allen, M.; Pinto, J. P. *Astrophys. J. Suppl. Ser.* **1984**, *55*, 465.
(12) Coustenis, A. *Ann. Geophys.* **1990**, *8*, 645.
(13) Coustenis, A.; Bezard, B.; Gautier, D.; Marten, A.; Samuelson, R. *Icarus* **1991**, *89*, 152.
(14) Bezard, B.; Marten, A.; Paubert, G. *Bull. Am. Astron. Soc.* **1993**, *25*, 1100.
(15) Nizamov, B.; Leone, S. R. *J. Phys. Chem. A* **2004**, *108*, 1746.
(16) Hoobler, R. J.; Leone, S. R. *J. Geophys. Res. [Planets].* **1997**, *102*, 1816.
(17) Vakhtin, A. B.; Lee, S.; Heard, D. E.; Smith, I. W. M.; Leone, S. R. *J. Phys. Chem. A* **2001**, *105*, 7889.
(18) Vakhtin, A. B.; Heard, D. E.; Smith, I. W. M.; Leone, S. R. *Chem. Phys. Lett.* **2001**, *344*, 317.
(19) Vakhtin, A. B.; Heard, D. E.; Smith, I. W. M.; Leone, S. R. *Chem. Phys. Lett.* **2001**, *348*, 21.
(20) Murphy, J. E.; Vakhtin, A. B.; Leone, S. R. *Icarus* **2003**, *163*, 175.
(21) Hoobler, R. J.; Leone, S. R. *J. Phys. Chem. A* **1999**, *103*, 1342.
(22) Lee, S.; Leone, S. R. *Chem. Phys. Lett.* **2000**, *329*, 443.
(23) Opansky, B. J.; Leone, S. R. *J. Phys. Chem.* **1996**, *100*, 4888.
(24) Opansky, B. J.; Leone, S. R. *J. Phys. Chem.* **1996**, *100*, 19904.
(25) Pedersen, J. O. P.; Opansky, B. J.; Leone, S. R. *J. Phys. Chem.* **1993**, *97*, 6822.

(26) Hu, W. P.; Truhlar, D. G. *J. Am. Chem. Soc.* **1996**, *118*, 860.
(27) Truhlar, D. G.; Carrett, B. C. *Acc. Chem. Res.* **1980**, *13*, 440.
(28) Truhlar, D. G.; Isaacson, A. D.; Garrett, B. C. Generalized Transition State Theory. In *Theory of Chemical Reaction Dynamics*; Baer, M., Eds.; CRC Press: Boca Raton, FL, 1985; p 65.
(29) Truhlar, D. G.; Garrett, B. C. *Annu. Rev. Phys. Chem.* **1984**, *35*, 159.
(30) Becke, A. D. *J. Chem. Phys.* **1993**, *98*, 1372.
(31) Lee, C.; Yang, W.; Parr, R. G. *Phys. Rev. B* **1988**, *37*, 785.
(32) Fast, P. L.; Truhlar, D. G. *J. Phys. Chem. A* **2000**, *104*, 6111.
(33) Frisch, M. J.; Trucks, G. W.; Schlegel, H. B.; Scuseria, G. E.; Robb, M. A.; Cheeseman, J. R.; Zakrzewski, V. G.; Montgomery, J. A., Jr.; Stratmann, R. E.; Burant, J. C.; Dapprich, S.; Millam, J. M.; Daniels, A. D.; Kudin, K. N.; Strain, M. C.; Farkas, O.; Tomasi, J.; Barone, V.; Cossi, M.; Cammi, R.; Mennucci, B.; Pomelli, C.; Adamo, C.; Clifford, S.; Ochterski, J.; Petersson, G. A.; Ayala, P. Y.; Cui, Q.; Morokuma, K.; Salvador, P.; Dannenberg, J. J.; Malick, D. K.; Rabuck, A. D.; Raghavachari, K.; Foresman, J. B.; Cioslowski, J.; Ortiz, J. V.; Baboul, A. G.; Stefanov, B. B.; Liu, G.; Liashenko, A.; Piskorz, P.; Komaromi, I.; Gomperts, R.; Martin, R. L.; Fox, D. J.; Keith, T.; Al-Laham, M. A.; Peng, C. Y.; Nanayakkara, A.; Challacombe, M.; Gill, P. M. W.; Johnson, B.; Chen, W.; Wong, M. W.; Andres, J. L.; Gonzalez, C.; Head-Gordon, M.; Replogle, E. S.; Pople, J. A. Gaussian 98 (revision A. 7); Gaussian, Pittsburgh, PA, 2001.
(34) Chang, Y.-Y.; Corchado, J. C.; Fast, P. L.; Villa, J.; Hu, W. -P.; Liu, Y, -P.; Lynch, G. C.; Jackels, C. F.; Nguyen, K. A.; Gu, M. Z.; Rossi, I.; Coitino, E. L.; Claylon, S.; Melissas, V. S.; Lynch, B. J.; Steckler, R.; Garrett, B. C.; Isaacson, A. D.; Truhlar, D. G. POLYRATE version 8. 4 0.1; University of Minnesota, Minneapolis, MN, 2000.
(35) Liu, Y.-P.; Lynch, G. C.; Truong, T. N.; Liu, D.-H.; Truhlar, D. G.; Garrett, B. C. *J. Am. Chem. Soc.* **1993**, *115*, 2408.
(36) Steckler, R.; Hu, W.-P.; Liu, Y.-P.; Lynch, G. C.; Garrett, B. C.; Isaacson, A. D.; Melissas, V. S.; Lu, D.-P.; Troung, T. N.; Rai, S. N.; Hancock, G. C.; Lauderdate; J. G, *Comput. Phys. Commun.* **1995**, *88*, 341.
(37) IUPAC, http://www.iupac.org/reports/1999/7110minkin/i.html.
(38) Linstrom, P. J.; Mallard, W. G., Eds. NIST Chemistry WebBook, 2005; http://webbook.nist.gov/chemistry/.
(39) Chuang, Y. Y.; Corchado, J. C.; Truhlar, D. G. *J. Phys. Chem.* **1999**, *103*, 1140.

JP804010T